Progress in Physics of Applied Materials 3 (2023) 147–158

Semnan University

Progress in Physics of Applied Materials

journal homepage: https://ppam.semnan.ac.ir/

Chitosan - Carbon Nanotube - Maghemite nanocomposites – A Flexible Negative Dielectric Constant Material

Annamalai Saravanan[a], Radha Perumal Ramasamy[b]*

[a] *Department of Physics, Bharath Institute of Higher education and Research, Chennai – 600 073, INDIA*
[b] *Department of Physics, CEG Campus, Anna University, Chennai – 600 025, INDIA*

ARTICLE INFO

Article history:
Received: 30 August 2023
Revised: 17 December 2023
Accepted: 18 December 2023

Keywords:
negative dielectric constant materials
chitosan
carbon nano tubes
maghemite

ABSTRACT

In this work, the nanocomposites of chitosan containing carbon nanotubes (CNT) and maghemite nanoparticles have been prepared by solution casting method. Techniques such as Raman spectroscopy, SEM, TEM, dielectric relaxation spectroscopy, and VSM studies were made. The incorporation of CNT in to the chitosan matrix and also the interaction between the CNT and the maghemite nanoparticles were studied using Raman spectroscopy. The dielectric constant of Chitosan-CNT composites turned from positive to negative at low frequency when CNT concentration increased from 10 to 20wt%. Interestingly, addition of 20wt% of maghemite nanoparticles into the Cs-CNT nanocomposites affected both the dielectric property and the conductivity of the composite. VSM measurement shows that the prepared maghemite nanoparticles and the Cs-CNT-maghemite nanocomposites are superparamagnetic materials. Observed dielectric characteristics and the electrical conductivity of the samples have been explained by using a model. Tuning of negative permittivity in the chitosan-CNT nanocomposites by using maghemite nanoparticles could be useful as metamaterials.

1. Introduction

Currently, metamaterials are studied extensively due to their unique electromagnetic behavior such as negative permittivity, negative permeability, negative refractive index, reversed Chrenkov radiation, and reversed Doppler effect [1]. It has wide range of application in field of super lens, wave filter, and improvement of antenna performance [2-4]. It is also used for producing new functionalities such as the cloak for invisibility [5]. The negative dielectric constant characteristics of the metamaterial is observed from the special structures of the materials [6]. Recently, the polymer nanocomposites (PNC) have been explored as metamaterial [7].

The phenomenon of negative permittivity was observed in CNT [8]. Carbon nanotubes (CNTs) have been considered as one of the effective filler materials for the polymer matrix due to their high electrical conductivity, thermal conductivity, and high mechanical strength [9]. Carbon nanotube filled polymers has applications such as in transparent conductive coatings, electrostatic dissipation, electrostatic painting, and EMI shielding applications [10]. In the polymer nanocomposite, at the percolation threshold limit, CNTs approach each other within several nanometers and forms a continuous conductive network inside the polymer matrix which leads to the efficient electron transfer between the nanotubes [11]. Enhancement of electrical conductivity has been observed in carbon nanofiber /polytherimide composite membranes when the carbon nanofiber loading reaches the percolation threshold limit and it leads to the negative permittivity [12].

Chitosan is the second most abundant naturally occurring biopolymer after cellulose, which has been shown to be a biocompatible, low-cost, and smart polymer material with excellent film forming ability [13]. It is an important material in the field of advanced sensor technology [14].

* Corresponding author. Tel.: 08608762302
E-mail address: perumal.ramasamy@gmail.com

Cite this article as:
Saravanan A. and Radha Perumal Ramasamy R.P., 2023. Chitosan - Carbon Nanotube - Maghemite nanocomposites – A Flexible Negative Dielectric Constant Material. *Progress in Physics of Applied Materials*, *3*(2), pp.147-158. DOI: 10.22075/PPAM.2023.31641.1064

Chitosan is also a good polymeric dispersant for carbon nanotubes in acetic acid [15]. Chitosan solution prepared using acetic acid contains protonated $-NH^{3+}$ group and the nanotubes interacts with the chitosan through this $-NH^{3+}$ group [16]. Chitosan-carbon nanotubes nanocomposites have wide range of applications such as electrochemical actuators and biosensor [17]. Magnetic iron oxide nanoparticles, especially maghemite have been studied for a long time, because of their interesting magnetic properties (superparamagnetism and strong magnetic response under external magnetic fields), easy availability, biocompatibility, and low cost. They have wide range of applications in spintronics, catalysis, biomedicine, and as constituents for biosensors [18]. Maghemite has ferrimagnetic behavior at room temperature. When its size is reduced below certain critical limit, it exhibits superparamagnetic (SPM) behavior associated with the formation of a single-domain state [19]. Polypyrrole-iron oxide nanoparticles have shown negative permittivity [20]. In this research we report the dielectric characteristics of chitosan- CNT- maghemite nanocomposites.

2. Experimental

All reagents used in the experiment were analytical grade and used as received without further purification. Chitosan powder (99.9% purity) and acetic acid (99.9% purity) were purchased from SRL Pvt. Ltd, Mumbai, India. Iron nitrate nonahydrate ($FeNO_3.9H_2O$ - 98% purity) and ammonium hydroxide solution were purchased from Merck Specialities Pvt Ltd, Mumbai, India. The Ferrous sulphate heptahydrate ($FeSO_4.7H_2O$- 98% purity) was purchased from RFCL Limited, New Delhi, India. Deionised water was used throughout the experiments. CNT (multiwalled) with carbon content > 99% was purchased from Sigma-Aldrich.

2.1. Preparation of γ-Fe_2O_3 nanoparticles

Iron oxide nanoparticles were prepared by a co-precipitation method [21]. A stoichiometric mixture of $FeSO_4.7H_2O$ (0.1M) and $FeNO_3.9H_2O$ (0.2M) in an aqueous solution was stirred for 30 minutes using magnetic stirrer at room temperature to obtain homogeneous solution and 0.3M of NH_3OH solution was added to the mixture drop by drop until formation of black precipitate. The precipitation was formed at a pH between 8 and 14. Formed black precipitate was collected and centrifuged five times by giving alternate wash with distilled water, acetone, and ethanol. Finally, the precursor was kept in oven at 100˚C for 12hr. The obtained black powder was sintered at 300˚C for 2hr to get the light brown γ-Fe_2O_3 nanoparticles.

2.2. Preparation of Chitosan-CNT nanocomposites

First, the chitosan solution was prepared by adding chitosan powder (1 wt%) in to the aqueous acetic acid solution (200 mL, 1.5 wt%). The mixture was stirred using magnetic stirrer and heated at 60°C temperature for 30–45 min. After complete dissolving of the chitosan powder, a semitransparent thick solution was obtained. Series of chitosan-CNT nanocomposites were prepared by adding an appropriate amount of CNT (10, 20 and 30 wt%) into the chitosan solution and it was ultrasonicated for 30 min for complete dispersion of CNT into the chitosan solution. The mixture was poured into Petri dish for drying. Finally, the chitosan containing 10, 20, and 30 wt % of CNT were labelled as Cs-10%CNT, Cs-20%CNT, and Cs-30%CNT, respectively.

2.3. Preparation of Chitosan-CNT-γ-Fe_2O_3 nanocomposites

Appropriate amount maghemite nanoparticles (20 wt%) were added into each of the chitosan-CNT solution having varying concentration of CNT (10-30wt%) and it was ultrasonicated for 30 min for complete dispersion of maghemite into the chitosan- CNT solution. The mixture was poured into Petri dish for drying. The obtained films were labelled as Cs-10%CNT-20%γ-Fe_2O_3, Cs-20%CNT-20% γ-Fe_2O_3 and Cs-30%CNT-20% γ-Fe_2O_3.

3. Characterization

The Raman spectra were obtained by using Confocal scanning spectrometer (Renishaw InVIA) with 532 nm argon ion laser excitation from 100cm^{-1} to 2000 cm^{-1} at room temperature. The surface morphology of the samples was characterized by using High resolution scanning electron microscopy (FEI Quanta FEG 200). HRTEM imaging was carried out using TECNAI T30 G2 STWIN with the operating voltage of 250kV. The HRTEM samples were prepared by drying drop of the water suspension on carbon-coated copper TEM grids. The ac conductivity and the dielectric properties were measured at room temperature using Novocontrol GmBH Concept 40 Broadband Dielectric Spectrometer (Novocontrol Technologies, Germany) in the frequency range of 0.1 Hz to 10 MHz at ac electric signal of 1 volt. The samples were used in the form of circular films with a diameter of 2cm and thickness of 60-80 μm. The samples were kept in-between two gold coated circular Cu plate electrodes, one of which was spring-loaded to maintain good electrical contact with the sample and the measured data was collected using WinDETA software. Magnetic measurements were carried out by using Superconducting Quantum Interference Device - Vibrating Sample Magnetometer (SQUID-VSM) (Quantum design, USA) at room temperature in the field range from -70000 Oe to 70000 Oe.

4. Results and discussion

4.1. Spectroscopy and imaging studies

4.1.1. Raman measurements

Raman spectroscopy is a powerful tool to evaluate the interfacial interaction between carbon-based materials and the polymer. Figure 1 shows the Raman spectra for chitosan film, γ -Fe_2O_3 nanoparticles and Cs-20%γ-Fe_2O_3. Chitosan film (Figure 1a) does not show any Raman peaks. It is due to low scattering cross-section of chitosan. Figure 1b shows Raman peaks for γ-Fe_2O_3 at 296, 394, 499, and broad peak at 695 cm^{-1}. It is reported that the characteristic peaks of inverse spinel structure of γ -Fe_2O_3 corresponds to 350, 500, and 700 cm^{-1} [22]. The broad peak around 700

cm^{-1}, correspond to the characteristic peak of γ-Fe_2O_3 [23]. The Raman peaks for Cs-20%γ-Fe_2O_3 (Figure 1c) are observed at 299,386,481, and 654 cm^{-1} which indicate the incorporation of γ-Fe_2O_3 nanoparticles into the chitosan matrix. Figure 2 shows the Raman spectra for CNT and the nanocomposites of Cs-CNT and Cs-CNT-γ-Fe_2O_3 films. The Raman spectrum of CNT (Figure 2a) shows two characteristic peaks centered at 1313 and 1583 cm^{-1}, respectively which corresponds to the D and G bands of graphite. The peak at 1313 cm^{-1} is assigned to D band (A_{1g} symmetry) representing edge induced disordered graphite structures and the peak at 1583 cm^{-1} is assigned for G band (E_{2g} symmetry, graphite mode) associated with tangential C-C band stretching motion originated from the E_{2g2} mode at 1580 cm^{-1} in graphite [24]. On addition of CNT in to the chitosan, the D as well as G band peak was blue shifted. The blue shift of the D and G band indicates the effect of interaction between the chitosan and CNT [25]. The Raman shift and the corresponding ID/IG intensity ratio values are tabulated in the Table.1. When 20 wt% γ-Fe_2O_3 nanoparticles were added in to the Cs-CNT composites, the G band is red shifted. It indicates the strong interaction between the CNT and γ-Fe_2O_3 nanoparticles in the chitosan matrix. Similar kind of red shift behavior of G band has been reported for the graphene containing iron oxide nanoparticles [26]. The Raman intensity ratio of the D and G bands (ID/IG) are related to the density of defects in the carbon materials as well as the edge smoothness and the edge structures [27]. The intensity of the D band is higher than that of the G band for all the samples, indicating a high concentration of disordered carbon present in the sample. The ID/IG ratio of the CNT is found to be 1.564. The ID/IG ratio of Cs-10% CNT, Cs-20% CNT, and Cs-30% CNT was found to be 1.153, 1.121, and 1.168, respectively. The decrease in the intensity ratio of Cs-CNT composites (as compared to the CNT) is possibly due to interaction between CNT's defects and chitosan. Figure 2 (e-g) shows the Raman spectra for Cs-CNT nanocomposites containing 20wt% of γ-Fe_2O_3 nanoparticles. No traces of γ-Fe_2O_3 nanoparticles peaks were observed, however the incorporation of γ-Fe_2O_3 nanoparticles in the Cs-CNT shows enhancement in the Raman intensity ratio. The ID/IG ratio of Cs-20%γ-Fe_2O_3 containing 10, 20, and 30 wt% CNT was observed to be 1.202, 1.158, and 1.181, respectively. The slight increase in the value of ID/IG indicates that γ-Fe_2O_3 nanoparticles could induce some additional defects in CNTs in the chitosan matrix [28].

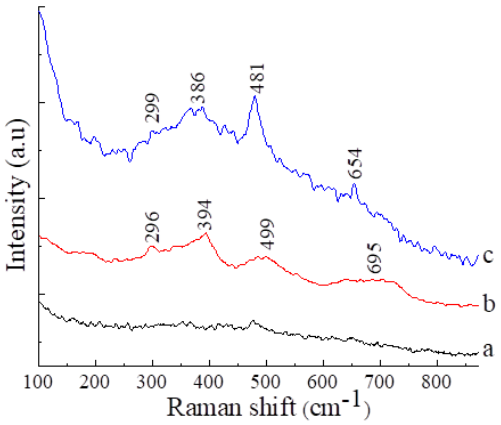

Fig. 1. Raman spectra of a) Chitosan film b) γ - Fe_2O_3 nanoparticles and c) Cs-20%γ-Fe_2O_3.

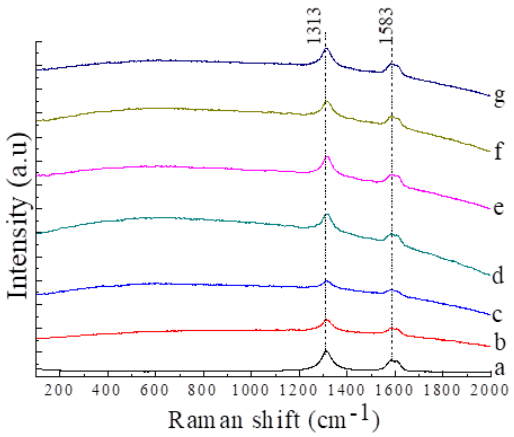

Fig. 2. Raman spectra of a) CNT, b) Cs-10% CNT, c) Cs-20% CNT, d) Cs-30% CNT, e) Cs-10% CNT -20%γ-Fe_2O_3, f) Cs-20% CNT -20%γ-Fe_2O_3 and g) Cs-30% CNT -20%γ-Fe_2O_3.

4.1.2. FE-SEM measurements

Fig. 3 shows the surface microstructure of chitosan and the nanocomposites of chitosan containing 10 and 20 wt% of CNT. The surface of the chitosan film [Figure 3(A & B)] was observed to be crack free and smooth. Some small aggregates were observed in the film which is due to the undissolved chitosan powder. Cs-10%CNT [Figure 3 (C & D)] shows distribution of CNT throughout the chitosan matrix along with small aggregates. The size of CNT [Figure 3(D)] was found to be ~33 nm to ~81 nm. Cs-20% CNT [Figure 3(E&F)] shows uniform distribution of CNT throughout the chitosan matrix. It is also observed that the CNTs touched. The FE-SEM images for the Cs-10%CNT-20%γ-Fe_2O_3 [Figure 3(G&H)] and Cs-20%CNT-20% γ-Fe_2O_3 [Figure 3(I&J)] shows CNT inside the chitosan matrix. In order to clearly observe the presence of γ-Fe_2O_3 nanoparticles in the Cs-CNT matrix, HR-TEM measurements were taken.

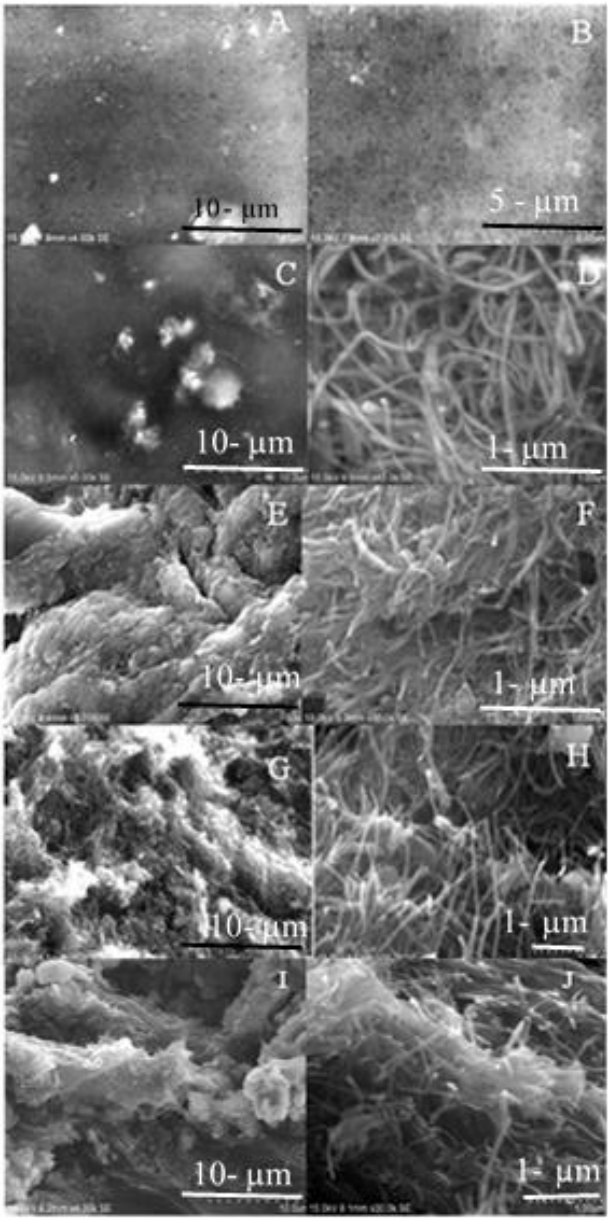

Fig. 3. FE-SEM images of (A) chitosan flim (B) chitosan flim (C) Cs-10% CNT, (D) Cs-10% CNT, (E) Cs-20% CNT, (F) Cs-20% CNT, (G) Cs-10%CNT-20%γ-Fe_2O_3, (H) Cs-10% CNT-20% γ-Fe_2O_3, (I) Cs-20% CNT-20% γ- Fe_2O_3 and (J) Cs-20% CNT-20% γ-Fe_2O_3.

4.1.3. HR-TEM measurement

The HR-TEM images of chitosan containing 10 wt% CNT and 20 wt% γ-Fe_2O_3 nanoparticles (Figure 4A) show some γ-Fe_2O_3 nanoparticles attached to the walls of the CNT and also dispersed in the chitosan film. The size of the nanoparticles was observed to be ~16 nm. The size of the individual CNT was found to be in the range of ~13nm to ~31nm. The size of the CNT observed from the FESEM measurements (33 nm to 81 nm) is different from HR-TEM measurements (13nm to 31nm). It is due to difference in their resolutions. In the film form, CNT was completely coated by the chitosan but in the solution form CNT can be individually seen. The electron diffraction image (Figure 4B) shows the diffused diffraction spots in the ring which is due to the presence of γ-Fe_2O_3 nanoparticles in the chitosan polymer. This result confirms the presence of γ-Fe_2O_3 nanoparticles and they are coated on side walls of CNT. Further, these coatings by maghemite nanoparticles could affect the dielectric properties. Hence the dielectric measurements were made and the results are as under.

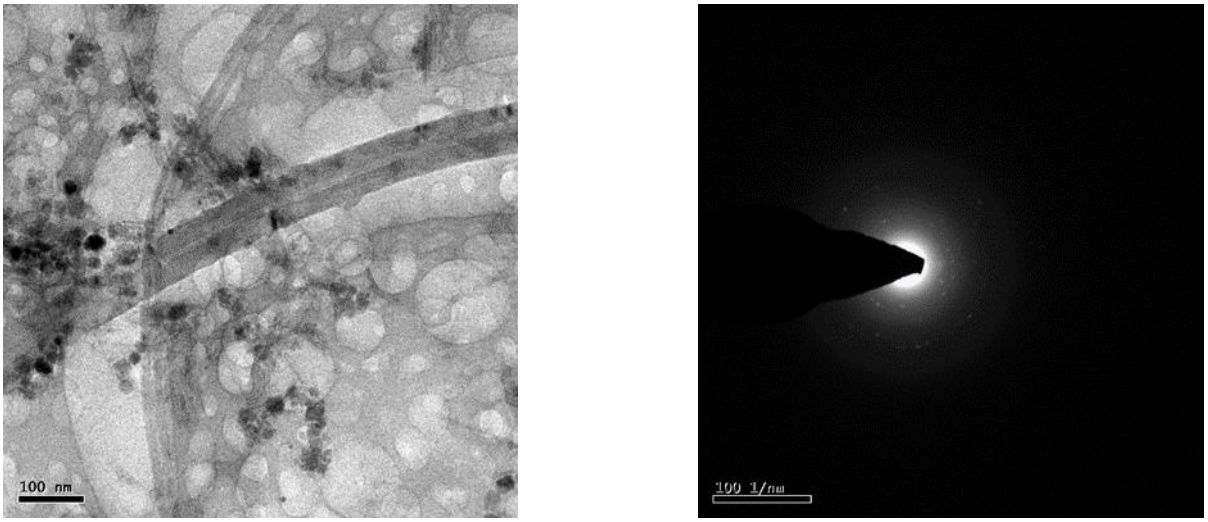

Fig. 4. HR-TEM images of A) Cs- 10% CNT-20% γ-Fe_2O_3 and corresponding B) selected area electron diffraction image (SAED).

4.2. Dielectric Studies

4.2.1. Dielectric Constant (ε')

Fig. 5A shows the frequency dependent variation of dielectric constant (ε') for γ-Fe_2O_3 nanoparticles, chitosan film, Cs-20%γ-Fe_2O_3, and the Cs-10%CNT. While the ε' of chitosan containing 10 % of CNT is positive in the frequency range 0.1 – 1 M Hz, the ε' of chitosan containing 20 and 30wt% of CNT (Figure 5B) shows negative values in the low frequency region and it becomes positive with increase in frequency. When the CNT content exceeds the percolation threshold limit, the CNTs approach each other and form conducting network of CNTs in the chitosan matrix. The dielectric constant becomes negative with the formation of conducting network of CNTs in the chitosan matrix. The frequencies at which the dielectric constant becomes 0 for Cs-20% CNT and Cs-30%γ-Fe_2O_3 are 5 and 11 Hz respectively. The effect of γ-Fe_2O_3 nanoparticles on the ε' of Cs/CNT nanocomposites with varying concentrations of CNT is shown in Figure 5(C). The ε' of the Cs-CNT-20% γ-Fe_2O_3 filled with 10, 20, and 30 wt% of CNT exhibits ε' values of -9.3, -27.3, and -48.5 at 1MHz, respectively. When increasing the CNT loadings in the Cs-CNT-γ-Fe_2O_3 nanocomposites large negative values of ε' were observed. The γ-Fe_2O_3 nanoparticles introduce lots of active interfaces between conductive CNT and nonconductive chitosan matrix within the composites. Under an electric field, a large number of charge carriers are accumulated at the interfaces and result in the sharp increase in permittivity, which is often called "Maxwell-Wagner-Sillars effect" [29]. Especially in the low frequency region, the dielectric constant of the Cs-CNT-γ-Fe_2O_3 nanocomposite showed enormously large negative values. The huge negative dielectric constant in the low frequency region can be due to accumulation of large number of γ-Fe_2O_3 nanoparticles around the CNTs in the chitosan matrix. For Cs-10% CNT-20%γ-Fe_2O_3, Cs-20% CNT-20%γ-Fe_2O_3, and Cs-30% CNT-20%γ-Fe_2O_3 the dielectric constant was negative in the measured frequency range (0.1-1 M Hz). The observed dielectric constant values at selected frequency for all the samples is listed in the Table.1.

4.2.2. *Dielectric loss (ε'')*

The Dielectric loss (ε'') indicates the energy loss of the material during the polarization [30]. Figure 6A shows the frequency dependent ε'' for chitosan film, γ-Fe_2O_3 nanoparticles, Cs-20%γ-Fe_2O_3, and Cs-CNT- maghemite nanocomposites. It is observed that the ε'' for all the samples decreased with increase in frequency. When the concentration of CNT reaches 20 wt%, the ε'' is enhanced abruptly. It is due to formation of continuous conducting network of CNTs in the chitosan matrix. The effect of 20 wt% of γ-Fe_2O_3 nanoparticles loading on the ε'' of Cs-CNT-maghemite nanocomposites is shown in Figure 6(B). Here also, the dielectric loss decreased with an increasing of frequency. The dielectric loss is increased with increasing the CNT from 10-30wt%. This is due to higher dissipation of heat by the CNTs. It orders to suppress the electrode polarization effect; electric modulus has been studied and is as follows.

4.2.3. Electric modulus studies

The real (M') and imaginary (M'') parts of the electrical modulus are obtained from the dielectric constant (ε') and dielectric loss (ε'') as follows.

$$M' = \varepsilon' / [\varepsilon'^2 + \varepsilon''^2] \quad (1)$$

$$M'' = \varepsilon'' / [\varepsilon'^2 + \varepsilon''^2] \quad (2)$$

Fig. 6 (C) gives the real part (M') of electric modulus with respect to frequency for the chitosan, γ-Fe_2O_3 nanoparticles, Cs-20%γ-Fe_2O_3, and Cs-CNT-maghemite nanocomposites. The M' plot for all the samples show a frequency independent behaviour up to 10^3 Hz and then it increases with increase in frequency. The frequency independent behaviour at low frequency is due to the high value of capacitance associated with the sample and it completely suppresses the electrode polarization effect [31]. The γ-Fe_2O_3 nanoparticles and Cs-20%γ-Fe_2O_3 show

the frequency independent behaviour up to 10^7 Hz. In the high frequency region, the value of M' decreases with an increasing concentration of CNT. Figure 6D shows the effect of γ-Fe_2O_3 loading on the M' of Cs-CNT composites containing varying concentration of CNT. The M' of all the sample shows frequency independent behaviour up to 10^3 Hz and then it increases with an increase in frequency. At high frequency region, the value of M' is decreased with an increase of CNT concentration from 10 to 30%. Figure 6 (E) shows the frequency dependent variations of imaginary part of the electric modulus (M'') for chitosan, γ-Fe_2O_3 nanoparticles, Cs-20%γ-Fe_2O_3, and the nanocomposites of Cs-CNT. Chitosan film shows the relaxation at ~2853 Hz and it is shifted towards high frequency with an increasing concentration of CNT. The relaxation peak shift towards high frequency indicates the enhancement of DC conductivity of the material. Similar kind of peak shift behaviour towards high frequency side was observed for the epoxy resin containing $BaTiO_3$ particles [32]. Figure 6F shows the effect of γ-Fe_2O_3 nanoparticles loading on the M'' of Cs-CNT nanocomposites containing varying concentration of CNT. The frequency independent behaviour of M'' of all the samples were observed up to 10^2 Hz. It is observed that as the CNT concentration increases the peak position shifts to the right indicating increase in conductivity, whereas when γ-Fe_2O_3 nanoparticles are incorporated the peak shifts to the left indicating decrease in conductivity.

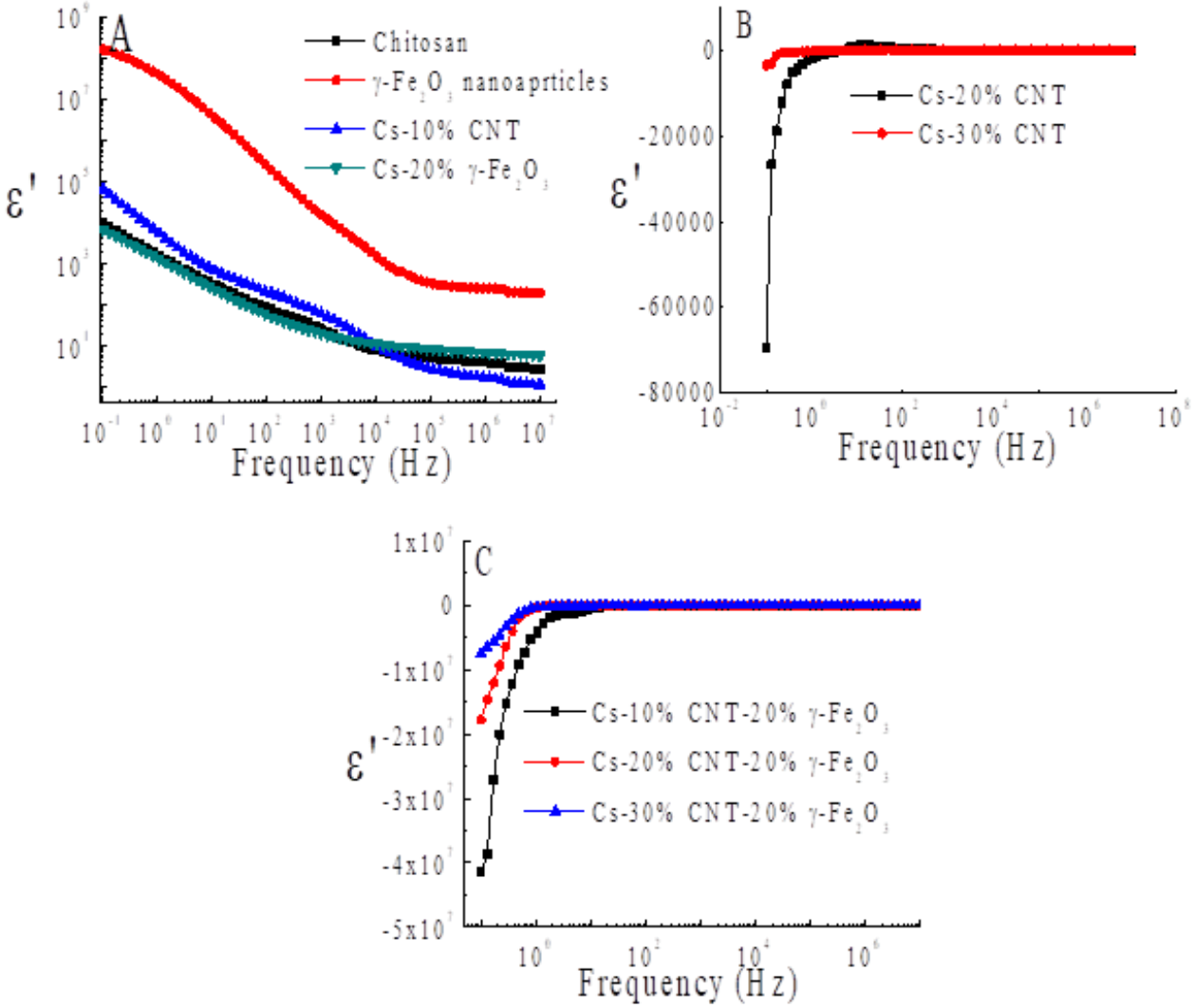

Fig.5. Frequency dependent plot for ε' of (A) chitosan, γ-Fe_2O_3 nanoparticles and Cs-10%CNT; (B) Cs/CNT nanocomposites; (C) Cs/CNT/γ-Fe_2O_3 nanocomposites.

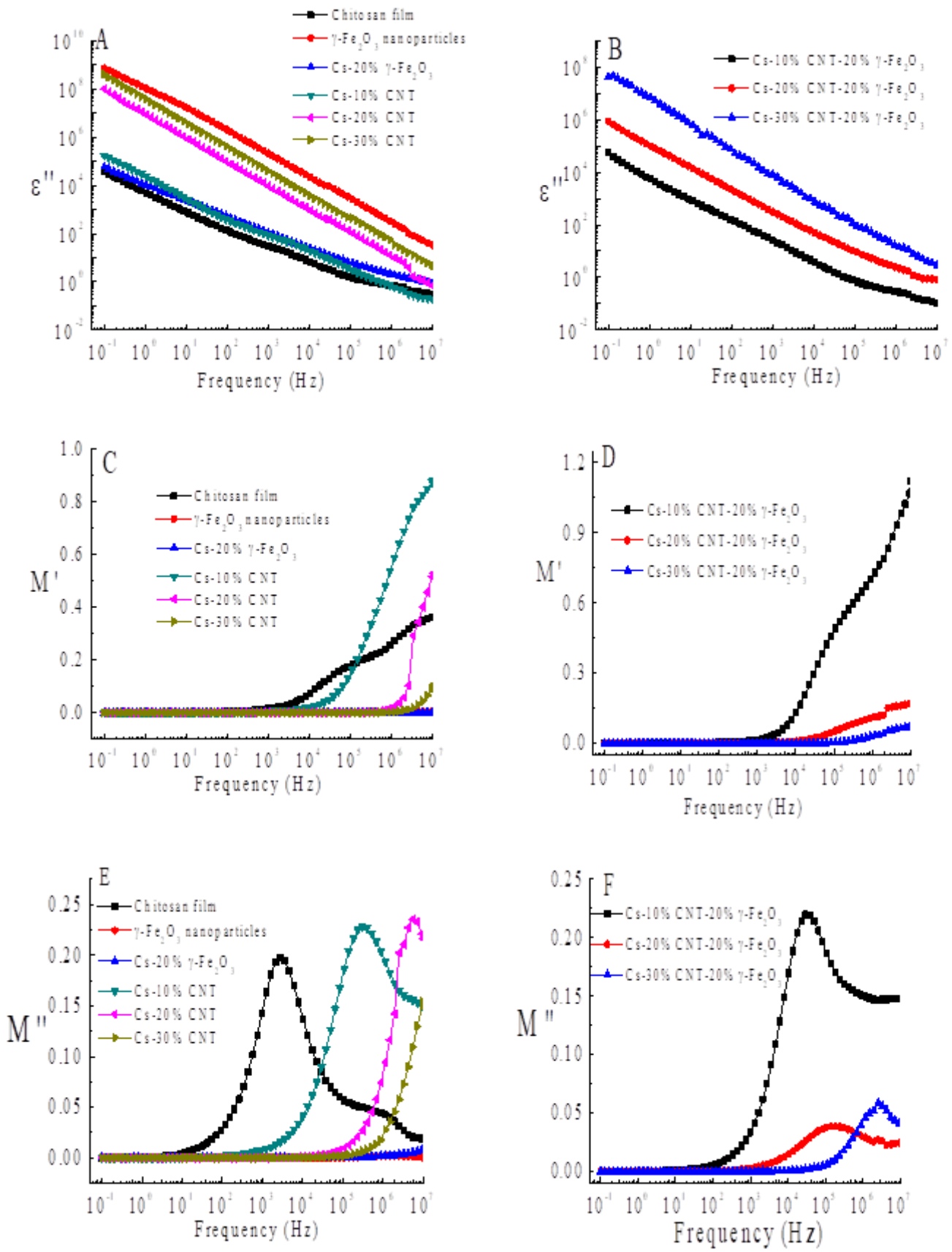

Fig.6. Frequency dependence plot of (A and B) ε'', (C and D) M' and (E and F) M'' for chitosan, γ-Fe_2O_3 nanoparticles and the nanocomposites.

Table 1. The dielectric permittivity (ε') values at selected frequencies.

S.No	Sample	ε' values at 0.1Hz	ε' values at 1KHz	ε' values at 1MHz
1.	Chitosan	9986	25	3.8
2.	γ-Fe_2O_3 nanoparticles	$1.6x10^8$	15521	248
3.	Cs-20%γ-Fe_2O_3	6573	19	6.4
4.	Cs-10% CNT	62810	60	1.6
5.	Cs-20% CNT	-69518	58	2.3
6.	Cs-30% CNT	-3494	11	9.8
7.	Cs-10% CNT-20%γ-Fe_2O_3	$-4.1x10^7$	-51	-9
8.	Cs-20% CNT-20%γ-Fe_2O_3	$-1.7x10^7$	-20	-27
9.	Cs-30% CNT-20%γ-Fe_2O_3	$-7.5x10^6$	-2192	-48

4.2.4. Electrical conductivity studies

Percolation model has been successfully applied to describe the electrical conductivity of Cs-CNT composite systems in which a distinct insulator to conductor transition is observed with an increasing concentration of CNT in the chitosan matrix [33]. Figure 7(A) shows the frequency dependence of electrical conductivity measured at room temperature for chitosan, γ-Fe_2O_3 nanoparticles, Cs-20%γ-Fe_2O_3, and the Cs-CNT nanocomposites. It is observed that the electrical conductivity (σ) of the chitosan film is increased with increase in concentration of CNT and exhibited an abrupt increase as the CNT content reached 20%. When the loading of CNT is less, the σ of the nanocomposite shows the frequency dependent behaviour which increased with frequency. However, the σ of nanocomposites drastically enhanced by several orders of magnitude as the CNT content increased to 20wt%. In a mixture between a dielectric (chitosan) and a conducting component (CNT), the conductivity of this mixture shows a critical behaviour if the fraction of the conducting component (CNT) reaches the percolation threshold [34]. Above the percolation threshold limit, the σ of composites rapidly increased due to the formation of an electrical conducting network of CNTs on the chitosan matrix. The effect of γ-Fe_2O_3 nanoparticles content on the electrical conductivity of Cs-CNT composites is shown in Figure 7B. Figure 7C shows the DC electrical conductivity measured at 0.1Hz for all the samples. It is observed that as the CNT concentration increases the conductivity also increases. Also, it is observed that γ-Fe_2O_3 reduces the conductivity. This is because γ-Fe_2O_3 nanoparticles may accumulate at the structural inter phase between the CNT and affect the electrical conductivity.

4.3. Magnetic studies

Fig. 8 shows the M-H curves of γ-Fe_2O_3 nanoparticles and Cs-CNT-20% γ-Fe_2O_3 contains varying concentration of CNT measured at room temperature. The hysteresis loops of all the samples were showing zero values of both coercivity (Hc) and remanent magnetization (M_R), indicating a superparamagnetic behaviour [35]. The saturation magnetization (Ms) of γ-Fe_2O_3 NP's (32.098 emu/g) is found to be lower than that of the reported bulk maghemite (76emu/g) [36]. It is because of the small size of γ-Fe_2O_3 nanoparticles (~16 nm) [37]. The M-H curve of chitosan film shows the diamagnetic behaviour with room temperature magnetization of ~ 0.0326 emu/g [38]. After subtracting the diamagnetic contribution, the saturation magnetization (Ms) of Cs-20% γ-Fe_2O_3 and Cs-CNT-20% γ-Fe_2O_3 with a CNT loading of 10, 20, and 30wt% were found to be 4.674, 4.534, 3.891, and 3.421 emu/g, respectively. It is observed that saturation magnetization (Ms) decreases with increasing the concentration of CNT. The saturation magnetization of polymer nanocomposites is found to be lower than that of the γ-Fe_2O_3 nanoparticles (32 emu/g). It is due to encapsulation of γ-Fe_2O_3 nanoparticles by chitosan.

4.4. Model

A model is shown in Figure 9. When 10wt % of CNT was added into the chitosan, no continuous conducting network of CNTs formed. The electrical conductivity is slightly higher than that of the chitosan film and the dielectric constant is observed to be positive. When increasing the CNT concentration from 10 to 20wt%, continuous conducting networks of CNTs formed in the chitosan matrix. The electrical conductivity is highly enhanced and

the dielectric constant was observed to be negative at low frequency. When the CNT content exceeds the percolation threshold limit, the CNTs are interconnected to each other and it leads to the higher level of charge delocalization. The delocalization of charge carriers in the interconnected CNTs in the chitosan matrix leads to the negative permittivity at low frequency. When 20 wt% of γ-Fe_2O_3 nanoparticles were added in to the Cs-CNT composite, its electric conductivity and the dielectric constant is modified. The electrical conductivity of Cs-CNT- γ-Fe_2O_3 was observed to be slightly less than that of the Cs-CNT because the conduction through CNT to CNT is high compared to the CNT - γ-Fe_2O_3- CNT in the chitosan matrix.

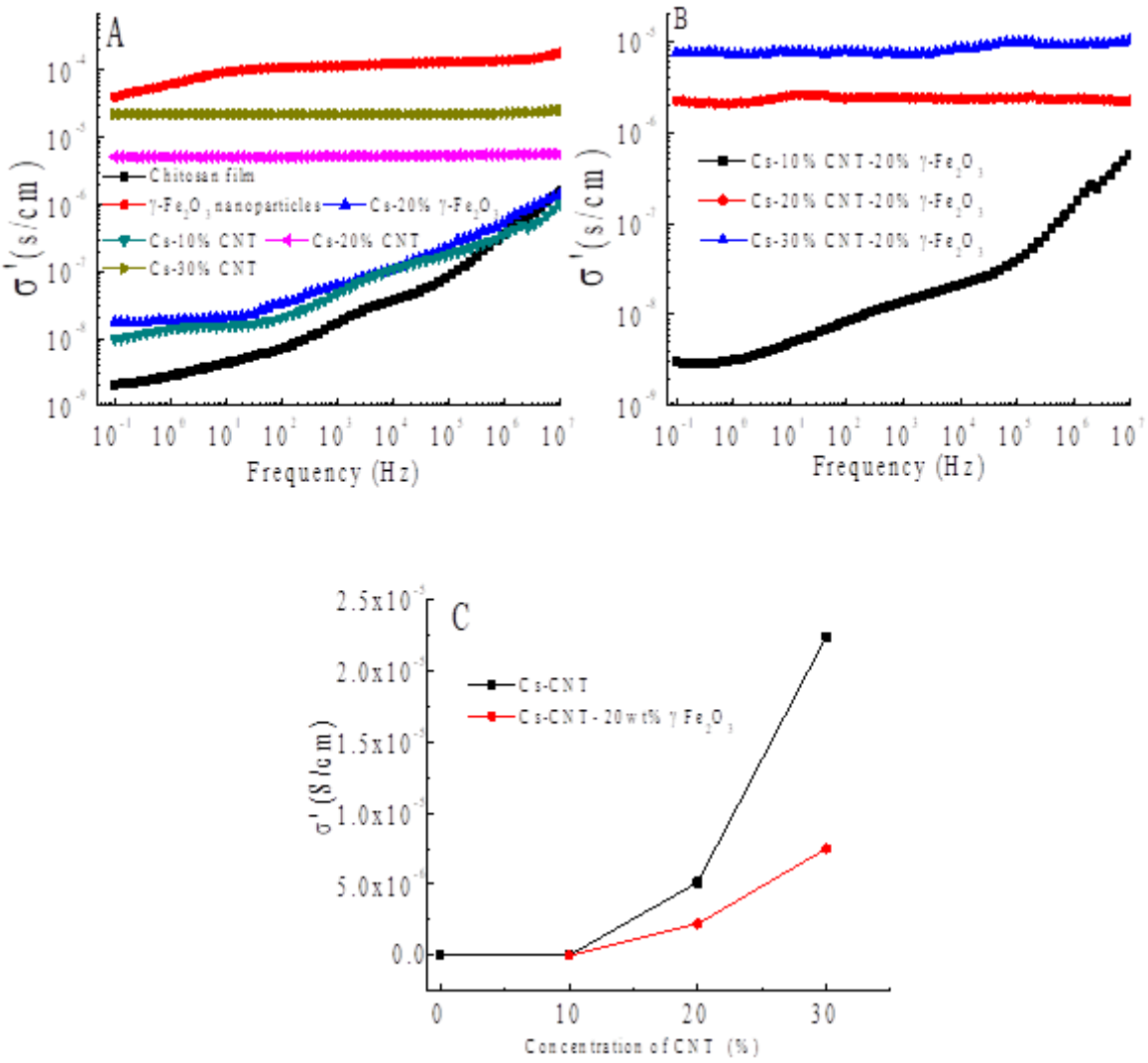

Fig.7. (A and B) Frequency dependence plot for electrical conductivity for chitosan, γ-Fe_2O_3 nanoparticles and the nanocomposites. (C) Dependence of DC conductivity (at 0.1 Hz) upon concentration of CNT and - nanoparticles in the nanocomposites at room temperature.

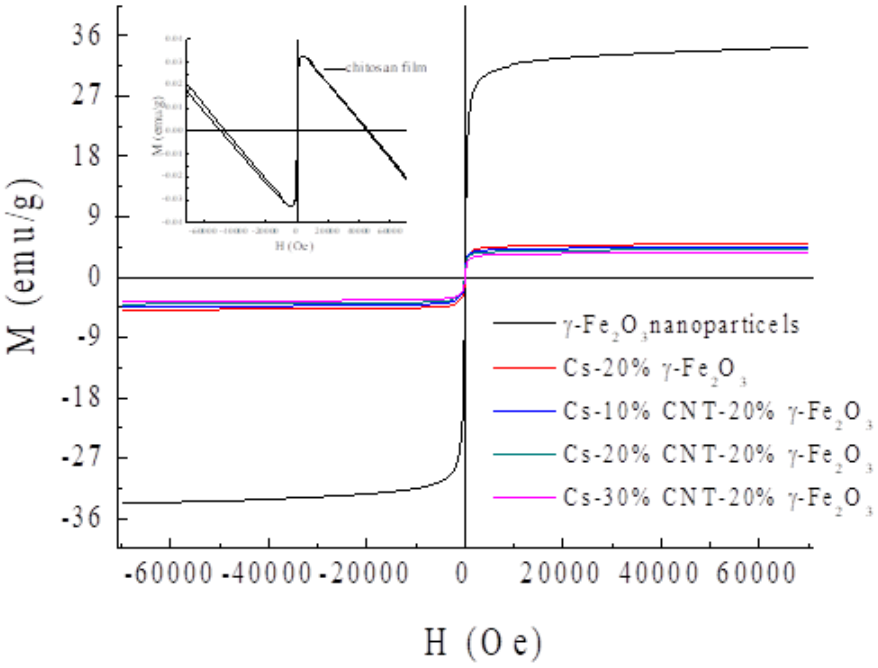

Fig. 8. Room temperature M-H curve for γ-Fe_2O_3 nanoparticles, Cs-20% γ-Fe_2O_3 and the nanocomposites of Cs/CNT/20%γ-Fe_2O_3 with CNT loading of 10, 20 and 30wt%, respectively. (Insect: M-H curve of chitosan film).

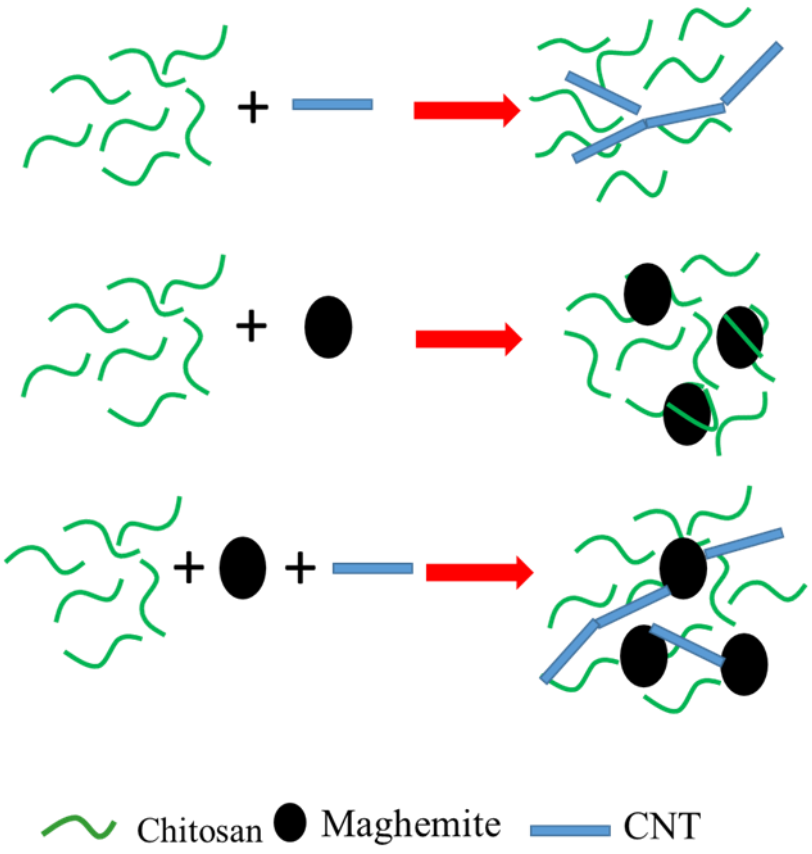

Fig. 9. Model for formation of Metacomposites

5. Conclusion

In this investigation, chitosan containing CNTs were prepared by a simple solution casting method. Negative permittivity behaviour was observed at low frequency when chitosan contained more than 20wt% of CNT. The electrical conductivity of the chitosan is transformed from insulating region to conducting region when the CNT content reached the percolation threshold limit. In that limit, continuous conducting networks were formed due to the interconnection of CNT. The delocalization of the charge carriers along the interconnected CNT networks leads to the negative permittivity. The relaxation peak of M'' was shifted to high frequency with an increasing loading concentration of CNT. The shifting of the relaxation peaks towards high frequency indicates enhancements of dc conductivity. Also, addition of γ-Fe_2O_3 nanoparticles in to the Cs-CNT decreased the electrical conductivity. Magnetic properties of synthesized γ-Fe_2O_3 nanoparticles and the PNC's of Cs-CNT-γ-Fe_2O_3 showed superparamagnetic behaviour. These materials could be very useful for the preparation and development of metacomposites.

Acknowledgements

The research was made possible due to funding provided by BRNS (DAE) India Sanction No 2011/37C/21/BRNS.

Conflicts of Interest

The author declares that there is no conflict of interest regarding the publication of this article.

References

[1] Smith, D.R., Pendry, J.B. and Wiltshire, M.C., 2004. Metamaterials and negative refractive index. *science*, *305*(5685), pp.788-792.

[2] Hoffman, A.J., Alekseyev, L., Howard, S.S., Franz, K.J., Wasserman, D., Podolskiy, V.A., Narimanov, E.E., Sivco, D.L. and Gmachl, C., 2007. Negative refraction in semiconductor metamaterials. *Nature materials*, *6*(12), pp.946-950.

[3] Pendry, J.B., Holden, A.J., Stewart, W.J. and Youngs, I., 1996. Extremely low frequency plasmons in metallic mesostructures. *Physical review letters*, *76*(25), p.4773.

[4] Dolgov, O.V., Kirzhnits, D.A. and Maksimov, E.G., 1981. On an admissible sign of the static dielectric function of matter. *Reviews of Modern Physics*, *53*(1), p.81.

[5] Cai, W., Chettiar, U.K., Kildishev, A.V. and Shalaev, V.M., 2007. Optical cloaking with metamaterials. *Nature photonics*, *1*(4), pp.224-227.

[6] Rockstuhl, C. and Lederer, F., 2007. Negative-index metamaterials from nanoapertures. *Physical Review B*, *76*(12), p.125426.

[7] Guo, J., Gu, H., Wei, H., Zhang, Q., Haldolaarachchige, N., Li, Y., Young, D.P., Wei, S. and Guo, Z., 2013. Magnetite–polypyrrole metacomposites: dielectric properties and magnetoresistance behavior. *The Journal of Physical Chemistry C*, *117*(19), pp.10191-10202.

[8] Zhang, Y., Yuan, S., Zhou, W., Xu, J. and Li, Y., 2007. Spectroscopic evidence and molecular simulation investigation of the π–π interaction between pyrene molecules and carbon nanotubes. *Journal of nanoscience and nanotechnology*, *7*(7), pp.2366-2375.

[9] Lau, C., Cooney, M.J. and Atanassov, P., 2008. Conductive macroporous composite chitosan– carbon nanotube scaffolds. *Langmuir*, *24*(13), pp.7004-7010.

[10] Kwon, J. and Kim, H., 2005. Comparison of the properties of waterborne polyurethane/multiwalled carbon nanotube and acid-treated multiwalled carbon nanotube composites prepared by in situ polymerization. *Journal of Polymer Science Part A: Polymer Chemistry*, *43*(17), pp.3973-3985.

[11] Coleman, J.N., Khan, U. and Gun'ko, Y.K., 2006. Mechanical reinforcement of polymers using carbon nanotubes. *Advanced materials*, *18*(6), pp.689-706.

[12] Sui, G., Li, B., Bratzel, G., Baker, L., Zhong, W.H. and Yang, X.P., 2009. Carbon nanofiber/polyetherimide composite membranes with special dielectric properties. *Soft Matter*, *5*(19), pp.3593-3598.

[13] Kumar, M.N.R., 2000. A review of chitin and chitosan applications. *Reactive and functional polymers*, *46*(1), pp.1-27.

[14] Suginta, W., Khunkaewla, P. and Schulte, A., 2013. Electrochemical biosensor applications of polysaccharides chitin and chitosan. *Chemical reviews*, *113*(7), pp.5458-5479.

[15] Takahashi, T., Luculescu, C.R., Uchida, K., Ishii, T. and Yajima, H., 2005. Dispersion behavior and spectroscopic properties of single-walled carbon nanotubes in chitosan acidic aqueous solutions. *Chemistry letters*, *34*(11), pp.1516-1517.

[16] Furtado, C.A., Kim, U.J., Gutierrez, H.R., Pan, L., Dickey, E.C. and Eklund, P.C., 2004. Debundling and dissolution of single-walled carbon nanotubes in amide solvents. *Journal of the American Chemical Society*, *126*(19), pp.6095-6105.

[17] Hu, Y., Chen, W., Lu, L., Liu, J. and Chang, C., 2010. Electromechanical actuation with controllable motion based on a single-walled carbon nanotube and natural biopolymer composite. *ACS nano*, *4*(6), pp.3498-3502.

[18] Sun, S., Murray, C.B., Weller, D., Folks, L. and Moser, A., 2000. Monodisperse FePt nanoparticles and ferromagnetic FePt nanocrystal superlattices. *science*, *287*(5460), pp.1989-1992.

[19] Lu, A.H., Salabas, E.E. and Schüth, F., 2007. Magnetic nanoparticles: synthesis, protection, functionalization, and application. *Angewandte Chemie International Edition*, *46*(8), pp.1222-1244.

[20] Kavas, H.Ü.S.E.Y.İ.N., Günay, M., Baykal, A., Toprak, M.S., Sozeri, H. and Aktaş, B., 2013. Negative permittivity of polyaniline–Fe_3O_4 nanocomposite. *Journal of Inorganic and Organometallic Polymers and Materials*, *23*, pp.306-314.

[21] Lee, S.J., Jeong, J.R., Shin, S.C., Kim, J.C. and Kim, J.D., 2004. Synthesis and characterization of superparamagnetic maghemite nanoparticles prepared by coprecipitation technique. *Journal of Magnetism and Magnetic Materials*, *282*, pp.147-150.

[22] Lee, K.J., An, J.H., Shin, J.S., Kim, D.H., Kim, C., Ozaki, H. and Koh, J.G., 2007. Protective effect of maghemite nanoparticles on ultraviolet-induced photo-damage in

human skin fibroblasts. *Nanotechnology*, *18*(46), p.465201.
[23] Kong, L., Yin, X., Zhang, Y., Yuan, X., Li, Q., Ye, F., Cheng, L. and Zhang, L., 2013. Electromagnetic wave absorption properties of reduced graphene oxide modified by maghemite colloidal nanoparticle clusters. *The Journal of Physical Chemistry C*, *117*(38), pp.19701-19711.
[24] Yang, C., Lin, Y. and Nan, C.W., 2009. Modified carbon nanotube composites with high dielectric constant, low dielectric loss and large energy density. *Carbon*, *47*(4), pp.1096-1101.
[25] Marroquin, J.B., Rhee, K.Y. and Park, S.J., 2013. Chitosan nanocomposite films: Enhanced electrical conductivity, thermal stability, and mechanical properties. *Carbohydrate polymers*, *92*(2), pp.1783-1791.
[26] Zhu, J., Luo, Z., Wu, S., Haldolaarachchige, N., Young, D.P., Wei, S. and Guo, Z., 2012. Magnetic graphene nanocomposites: electron conduction, giant magnetoresistance and tunable negative permittivity. *Journal of Materials Chemistry*, *22*(3), pp.835-844.
[27] Cheng, M., Yang, R., Zhang, L., Shi, Z., Yang, W., Wang, D., Xie, G., Shi, D. and Zhang, G., 2012. Restoration of graphene from graphene oxide by defect repair. *Carbon*, *50*(7), pp.2581-2587.
[28] Zhang, W., Li, X., Zou, R., Wu, H., Shi, H., Yu, S. and Liu, Y., 2015. Multifunctional glucose biosensors from Fe_3O_4 nanoparticles modified chitosan/graphene nanocomposites. *Scientific reports*, *5*(1), p.11129.
[29] Tamura, R., Lim, E., Manaka, T. and Iwamoto, M., 2006. Analysis of pentacene field effect transistor as a Maxwell-Wagner effect element. *Journal of applied physics*, *100*(11).
[30] Gevorgian, S.S., Tagantsev, A.K. and Vorobiev, A.K., 2013. *Tuneable film bulk acoustic wave resonators* (p. 2). London: Springer.
[31] Yakuphanoglu, F., 2007. Electrical conductivity and electrical modulus properties of α, ω-dihexylsexithiophene organic semiconductor. *Physica B: Condensed Matter*, *393*(1-2), pp.139-142.
[32] Ramajo, L., Reboredo, M. and Castro, M., 2005. Dielectric response and relaxation phenomena in composites of epoxy resin with $BaTiO_3$ particles. *Composites Part A: Applied science and manufacturing*, *36*(9), pp.1267-1274.
[33] Yousefi, N., Sun, X., Lin, X., Shen, X., Jia, J., Zhang, B., Tang, B., Chan, M. and Kim, J.K., 2014. Highly aligned graphene/polymer nanocomposites with excellent dielectric properties for high-performance electromagnetic interference shielding. *Advanced Materials*, *26*(31), pp.5480-5487.
[34] Efros, A.L. and Shklovskii, B.I., 1976. Critical behaviour of conductivity and dielectric constant near the metal-non-metal transition threshold. *Physica status solidi (b)*, *76*(2), pp.475-485.
[35] Chen, Y. and Gu, H., 2012. Microwave assisted fast fabrication of Fe_3O_4-MWCNTs nanocomposites and their application as MRI contrast agents. *Materials Letters*, *67*(1), pp.49-51.
[36] Millan, A., Urtizberea, A., Silva, N.J.O., Palacio, F., Amaral, V.S., Snoeck, E. and Serin, V., 2007. Surface effects in maghemite nanoparticles. *Journal of magnetism and magnetic materials*, *312*(1), pp.L5-L9.
[37] Rozman, M. and Drofenik, M., 1995. Hydrothermal synthesis of manganese zinc ferrites. *Journal of the American Ceramic Society*, *78*(9), pp.2449-2455.
[38] Bhatt, A.S., Bhat, D.K., Santosh, M.S. and Tai, C.W., 2011. Chitosan/NiO nanocomposites: a potential new dielectric material. *Journal of Materials Chemistry*, *21*(35), pp.13490-13497.